Accepted Manuscript

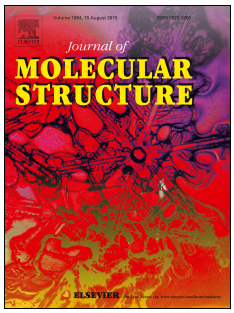

Synthesis, crystal structure, DFT calculations, Hirshfeld surface, vibrational and optical properties of a novel hybrid non-centrosymmetric material $(C_{10}H_{15}N_2)_2H_2P_2O_7$

Yathreb Oueslati, Sevgi Kansız, Arto Valkonen, Thameur Sahbani, Necmi Dege, Wajda Smirani

PII: S0022-2860(19)30833-6

DOI: https://doi.org/10.1016/j.molstruc.2019.06.110

Reference: MOLSTR 26752

To appear in: *Journal of Molecular Structure*

Received Date: 14 April 2019

Revised Date: 26 June 2019

Accepted Date: 29 June 2019

Please cite this article as: Y. Oueslati, S. Kansız, A. Valkonen, T. Sahbani, N. Dege, W. Smirani, Synthesis, crystal structure, DFT calculations, Hirshfeld surface, vibrational and optical properties of a novel hybrid non-centrosymmetric material $(C_{10}H_{15}N_2)_2H_2P_2O_7$, *Journal of Molecular Structure* (2019), doi: https://doi.org/10.1016/j.molstruc.2019.06.110.

Graphical abstract

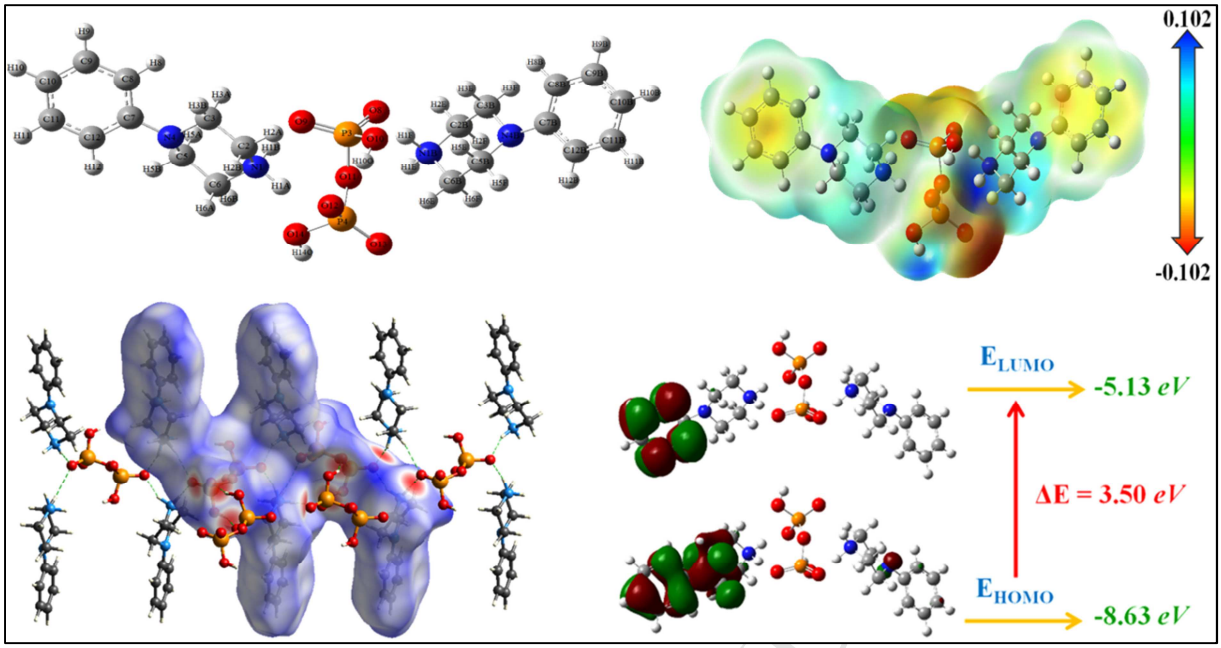

Synthesis, crystal structure, DFT calculations, Hirshfeld surface, vibrational and optical properties of a novel hybrid non-centrosymmetric material ($C_{10}H_{15}N_2)_2H_2P_2O_7$

Yathreb Oueslati[1], Sevgi Kansız[2], Arto Valkonen[3], Thameur Sahbani[1], Necmi Dege[2] and Wajda Smirani[1]

[1]*Laboratory of Chemical Materials, Faculty of Sciences of Bizerte, Carthage University, 7021 Zarzouna, Tunisia*
[2]*Department of Physics, Faculty of Arts and Sciences, Ondokuz Mayıs University, 55139, Samsun, Turkey*
[3]*Department of Chemistry, University of Jyvaskyla, 40014 Jyvaskyla, Finland*

Abstract

This present work undertakes the study of a novel organic–inorganic hybrid material, which has been obtained successfully by an acid-base reaction at room temperature and structurally studied by the single crystal X-ray diffraction method. $(C_{10}H_{15}N_2)_2H_2P_2O_7$ crystallizes in the triclinic system with the non-centrosymmetric space group P1 with the following lattice parameters: a = 5.9159(2) Å, b = 13.8451(6) Å, c = 14.5973(5) Å, α = 74.507(2)°, β= 89.980(2)°, γ = 89.231(2)° with V = 1152.06(8) $Å^3$ and Z = 2. The X-ray structural analysis supported by a detailed Hirshfeld 2D fingerprint plots has been performed to elucidate the different inter-contacts in the crystal structure mainly associated with N-H···O, O-H···O and C-H···O between the different entities. An infrared spectrum was registered to reveal the vibrational modes of the title compound. The optical measurements have been carried out at room temperature. Theoretical calculations, which are quantum chemical techniques, based in density functional theory (DFT) method in the ground state will be devoted to study the vibrational frequencies and structural parameters of the investigated molecule by using DFT/B3LYP/6-311G(d,p) basis set. The calculated geometric parameters and vibrational frequencies are in good line with their experimental data.

Keywords: Non–centrosymmetric hybrid material; Crystal structure; DFT; MEP; Mulliken charges; HOMO-LUMO.

1. Introduction

Nowadays, a remarkable interest is bringing to the organic-inorganic hybrid materials. Among this large family, the main focus was on the hybrid compounds based on phosphates, in particular. The need to use these materials, which gather the best properties of both the organic and the inorganic components in a single phase, is permanently increasing. Hence, this symbiosis can lead to new rich structure, chemical and physical properties and has secured a good place in various fields of application such as biomolecular science [1,2], electronic [3], nonlinear optics [4-6] and medicine, where $C_{15}H_{23}N_3O_2(H_2PO_4)_2$ have been found to have the potential for treatment of malaria [7]. In this context, the phosphate anion

has been combined with an organic amine based on piperazine that is used as structure directing agents due to their important characteristics.

Moreover, phenylpiperazine and its derivates are widely employed as an organic cation owing to their excellent biological, pharmacology and cardiovascular properties. In this regard, it has been noticed that piperazine derivates are very often found in a plethora of well-known drugs with various therapeutic uses, such as antipsychotic [8-10], anticancer [11], antifungal, antibacterial, antihistaminic and antidepressant.

Much attention is currently devoted to the non-centrosymmetric structures of organic cation diphosphates which are still limited in comparison with other centrosymmetric diphosphates [12,13]. In fact these compounds are potentially applicable as nonlinear optical materials (NLO). Indeed, such compounds is of enormous technological importance and embrace a wide variety of active field of research due to their potential applications in telecommunications, electro-optical shutters, terahertz (THz) imaging and spectroscopy, optical data storage and optical information processing [14]. Furthermore, the key that make the non-centrosymmetric crystals one of the most intensively studied compounds is their important nonlinear property called ″Second Harmonic Generation″ which has been performed by Franken and co-workers since 1960 [15]. This process is also called frequency doubling where incident photons with a frequency ω interacting with a nonlinear material are directly converted into new photons with twice the frequency 2ω of the initial one [16].

To gain insight into the structural characterization of the novel compound, 1-phenylpiperazinium dihydrogenodiphosphate $(C_{10}H_{15}N_2)_2H_2P_2O_7$, the present research work reports, the synthesis, the structure, the Hirshfeld surface analysis, the vibrational and the optical measurements. To calculate the theoretical geometry and IR spectrum of the title compound Density Functional Theory method was applied in gas phase. The molecular electrostatic potential (MEP), frontier orbitals (HOMO-LUMO) and Mulliken population analysis were obtained computationally. The B3LYP/6-311G(d,p) was chosen as basis set for the theoretical calculations.

2. Crystal growth and experimental techniques

The chemical synthesis of the title compound $(C_{10}H_{15}N_2)_2H_2P_2O_7$ via an acid-base reaction was carried out in two steps: Diphosphoric acid was first prepared by passing a solution of $Na_4P_2O_7$ through an ion exchange resin (Amberlite IR 120), and was immediately neutralized with an alcoholic solution of 1-phenylpiperazine. It should be noted that the organic molecule was added drop by drop with stirring for a few minutes until obtaining a final solution at pH 2. The resulting solution was then slowly evaporated over a few days at room temperature

until the appearance of good quality of colorless and transparent plate crystals occurred. The reaction scheme can be described as follows:

$$2(C_{10}H_{14}N_2) + H_4P_2O_7 \longrightarrow (C_{10}H_{15}N_2)_2H_2P_2O_7$$

A colorless crystal with approximate dimensions (0.25 x 0.22 x 0.04 mm^3) was selected in order to perform its structural analysis by X-ray diffraction. Bruker-Nonius Kappa CCD diffractometer with APEX II detector, employing graphite monochromated MoKα radiation (λ = 0.71073Å), was used to collect total reflections at temperature of 170 K. The structure was solved with SHELXT [17] and refined using SHELXL [18]. The drawing of the molecular structure was made with DIAMOND [19]. All non-hydrogen atoms were determined and refined isotropically and then anisotropically. All hydrogen atoms were situated in geometrically optimized positions and treated as riding atoms. Further details of the structure analysis are given in Table 1. Selected angles and bond lengths are presented in Table 2. The hydrogen bonds are listed in Table 3. The X-ray powder diffraction (XRPD) experiment was collected using a BRUKER D8-advance diffractometer with CuKα radiation (λ = 1.5406 Å) in the 2θ angular range from 0 to 40°.

The quantum chemical calculations and the molecular geometry optimization of $(C_{10}H_{15}N_2)_2H_2P_2O_7$ were performed using Gaussian03 program [20]. Subsequently, the calculation results were visualized with the Gauss-View4.1 [21]. Due to its cost-effectiveness, Density functional theory (DFT) with the Becke-three-parameter hybrid exchange functional combined with the Lee-Yang-Parr correlation functional (B3LYP) [22,23] levels with the standard 6-311G(d,p) basis set was used for complete calculations. To estimate the chemical reactivity of $(C_{10}H_{15}N_2)_2H_2P_2O_7$, the molecular electrostatic potential (MEP) surface map and Mulliken population analysis were obtained with theoretical calculations at the B3LYP/6-311G(d,p) level. In addition, the energies and FT-IR spectrum of optimized structure were also obtained at the same basis set. The harmonic vibration frequencies for the optimized structure were scaled using the scaling factor 0.9619 [24]. The molecular electrostatic potential (MEP) map, electrostatic potential contour map and frontier molecular orbitals (FMOs) were drawn using Gauss-View4.1 software.

To analyse the interactions in the crystal, Hirshfeld surfaces mapped with d_{norm} and their associated two-dimensional fingerprint presented in this paper were plotted using Crystal Explorer (version 3.1) software [25].

Infrared (IR) spectra were recorded at room temperature on a Nicolet IR200 FTIR equipped with a diamond micro-ATR access in the 4000–400 cm^{-1} range.

Solid state UV-Vis absorption spectra were obtained by a Perkin Elmer Lambda 35 spectrophotometer in the range of 200–800 nm.

Emission spectrum was obtained on a PerkinElmer LS55 fluorescence spectrometer equipped with a 450 W xenon lamp as the excitation source using solid sample at room temperature.

3. Results and discussions

3.1. Structure description

Fig.S1 compares the experimental and the simulated diffractograms recorded at room temperature of the synthesized product. It is noteworthy that the sample is in pure phase because both the XRPD pattern of the obtained material and the calculated pattern from the single crystal data are perfectly matched.

The ORTEP representation of the asymmetric unit of title compound shows two independent dihydrogenodiphosphates $H_2P_2O_7^{2-}$ anions and four 1-phenylpiperazinium cations $C_{10}H_{15}N_2^+$ (Fig.S2).

It is well observed in Fig.1a that the atomic arrangement of $(C_{10}H_{15}N_2)_2H_2P_2O_7$ is projected according to the (bc) plane. It shows that $[H_2P_2O_7]^{2-}$ anions are linked by O-H···O hydrogen bonds to built ribbons along the a axis at z = $\frac{1}{4}$ and z = $\frac{3}{4}$. These ribbons are interlinked through N-H···O hydrogen bonds to form a layer parallel to (bc) plane at y = $\frac{1}{2}$. Each anionic group is linked to its two close neighbors through four strong O-H···O hydrogen bonds, with an O···O distances between 2.524(7) and 2.599(7) Å. This association generates a single type of ring $R_2^2(8)$ (Fig.1b). The organic cations are located between the $[H_2P_2O_7]^{2-}$ anions and interconnected via N-H···O and moderate C-H···O hydrogen bonds forming a three-dimensional network.

Table 2 depicts the PO_4 distances inside the tetrahedral, indeed three main types of PO_4 distances are listed. The longest one P-O(L) corresponding to the P-O-P bonds which vary from 1.596(5)Å to 1.612(5)Å, the intermediate one, P-O(H), ranging from 1.528(5) to 1.540(5) and the shortest one, P-O(E), corresponding to the external oxygen atoms, which spread from 1.489(5) to 1.529(5). The average values for the P-O distances and O-P-O angles are (1.536(5)Å, 109.3(3)˚), (1.541(5)Å, 109.26(3)˚), (1.538(5)Å, 109.38(3)˚) and (1.541(5)Å, 109.29(3)˚) respectively for $P(1)O_4$, $P(2)O_4$, $P(3)O_4$ and $P(4)O_4$. The P-P distance is 2.94(3) Å and the P-O-P angle is 132.8(3)°. All these distances and angles are in agreement with previous structural informations about diphosphate anions [26]. The Baur method is a functional way to calculate the average values of the distorsion indices [27] corresponding to

the different angles and distances in the PO_4 tetrahedral which are presented in Table S1 [DI (OPO) = 0.034; DI (PO) = 0.020; and DI (OO) = 0.017].

It exhibits that the distortion in the P-O distances is slightly higher than O-O distances. Thereby, in this structure the PO_4 group form regular tetrahedral. The shape adopted by the four crystallographically independent organic cations shows the presence of two types of chair conformation, the most stable chemical conformation. The conformation of the piperazine six membered rings can be described in terms of Cremer & Pople puckering coordinates [28]. In the title compound, the puckering parameters of the four rings (N4-C5-C6-N1-C2-C3), (N4A-C5A-C6A-N1A-C2A-C3A), (N4B-C5B-C6B-N1B-C2B-C3B) and (N4C-C5C-C6C-N1C-C2C-C3C) are QT = 0.5527, q2 = 0.0196 q3 = 0.5524, θ = 2.03 φ = -29.17, QT = 0.5603, q2 = 0.0428 q3 = 0.5587, θ = 4.38 φ = 177.21, QT = 0.5566, q2 = 0.0176 q3 = 0.5563, θ = 1.81 φ = -8.96 and QT = 0.5670, q2 = 0.0507 q3 = 0.5647, θ = 5.13 φ = 173.75 respectively.

DFT calculations were applied on $(C_{10}H_{15}N_2)_2H_2P_2O_7$ at B3LYP/6-311G(d,p) level in order to estimate the effect of intermolecular interactions on geometrical parameters. The optimized structure of the compound is shown in Fig.2. The structural parameters obtained by the DFT method for the studied compound are given in Table 4 with experimental results. As shown, the optimized parameters (bond lengths, bond angles) are very close with the experimental data (Fig.S3). This slight difference can be explained by the fact that the calculation relates to the isolated molecule where the interaction with the neighboring molecules are absent, whereas the experimental result occurs in the solid state

3.2. Hirshfeld Surface analysis

Hirshfeld surface analysis is a powerful tool used to quantify the intermolecular interactions of molecular crystals. The Hirshfeld surfaces [29] and fingerprint plots [30] presented here are carried out using Crystal Explorer 3.1.The normalized contact distance (d_{norm}), based on d_e (distance from a point on the surface to the nearest nucleus outside the surface) and d_i (distance from a point on the surface to the nearest nucleus inside the surface), was calculated via the following expression:

$$d_{norm} = \frac{d_i - r_i^{vdW}}{r_i^{vdW}} + \frac{d_e - r_e^{vdW}}{r_e^{vdW}}$$

Where r_i^{vdW} is the van der Walls radius of the atom that lies inside the surface of Hirshfeld, while r_e^{vdW} is the van der Walls radius of the atom that lies outside of the surface of Hirshfeld.

The Hirshfeld surface of the title compound is illustrated in Fig.3. In this latter a color gradient is used, which varies from red (distances shorter than sum of vdW with negative d_{norm} value) through white (represents the contact around vdW separation with a d_{norm} value of zero) to blue (distance longer than of vdW with positive d_{norm} value). The red spots over Hirshfeld surface point out the inter-contacts included in hydrogen bonds [31,32]. It is well observed in Fig.3 that the red circular collapsing is attributed to O–H···O and N–H···O and C–H···O hydrogen-bonding interactions. The surfaces of 3D d_{norm} are plotted over a fixed color scale of -0.8042 (red) to 1.4147 (blue) Å with a standard (high) surface resolution.

The fingerprint plot of all the intermolecular contacts of the studied sample is shown in Fig.4a. This latter indicates that the highest contribution of total Hirshfeld surface is attributed to H···H interactions with 48.4% (Fig.4b) which arerepresented with a single broad peak at de = di ~ 1.1 Å, it should be also noted that (d_e+ d_i) ~ 2.2 Å. This value is superior to the sum of van der Waals radii of hydrogen atom (1.20 Å).

As can be seen the H···O/O···H contacts is considered as the second dominant interactions with 29.6% (Fig.4c) of the total Hirshfeld surface area which are appeared with two sharp symmetric spikes in the two-dimensional fingerprint maps. The value (d_e+ d_i) ~ 1.6 Å is less than the sum of van der Waals radii of oxygen (1.52 Å) and hydrogen (1.20Å) atoms. This result allows us to confirm that the inter-contact is considered as being close contact.

Other inter-contacts, H···C/C···H, H···N/N···H, C···C and P···H/H···P comprise 19.3%, 2.2%, 0.3% and 0.1% respectively.

3.3. IR Spectroscopy

FT-IR spectroscopy is considered as one of the powerful technique which was used to measure and identify the frequencies of vibrations of the bonds of the atoms making up the material, it is fair to note that every compound has a characteristic spectrum. In the present work, the theoretical IR spectrum was generated using the density functional theory (DFT) method with the B3LYP/6-311G(d,p) basis set on the optimized geometries of the compound. The scaling factor is taken as 0.9619 to reduce the discrepancy between the experimental frequencies and the computational methods. For visual comparison, the theoretical IR spectrum and the experimental one of $(C_{10}H_{15}N_2)_2H_2P_2O_7$ is reported in Fig.5. Table 5 presents the scaled calculated and experimental modes as well as the proposed assignments.

3.3.1. $H_2P_2O_7^{2-}$ Vibrations analysis

In the studied region, the symmetric and asymmetric stretching vibrations of the PO_3 terminal groups are located in the region 1256-988 cm^{-1}[33] and the DFT calculations give these

modes in the range 1248-1153 cm^{-1}. By analyzing Fig.5 the symmetric and asymmetric in plane bending vibrations, denoted as δ_s (PO_3) and δ_{as} (PO_3), are observed between 629 and 410 cm^{-1} [34]. The bands which appear between 760-692 cm^{-1} are assigned unambiguously to the symmetric stretching vibrations ν_s(POP), while that at 967 and 897 cm^{-1} are attributed to ν_{as}(POP) and POH modes. As seen from Table 5, the POP asymmetric stretching vibration are found at 844-785 cm^{-1} and the POP symmetric stretching vibration are appeared at 673 cm^{-1}.

3.3.2. $[C_{10}H_{15}N_2]^+$ cations vibrations

Generally, frequencies in the region 3100-3000 cm^{-1} are due to the stretching vibration ν(C-H) of aromatic ring. All the C-H bands are weak and this is due to the charge transfer between the hydrogen atoms and carbon atoms. The DFT computation predicts this vibrational mode around 3060 cm^{-1}. The theoretical value shows excellent agreement with the experimental value. The observed bands in the 2980-2208 cm^{-1} region can be assigned to symmetric and asymmetric stretching vibrations of $-CH_2$ and $-NH_2^+$. The stretching vibrations of N-H group occur in this same region. The peaks calculated as 2990 and 2932 cm^{-1} belong to the asymmetric and symmetric stretching vibration of the $-CH_2$ group. The C=C stretching vibration are generally observed at 1600-1400 cm^{-1}. In the present compound, the bands located between 1637-1398 cm^{-1} are ascribed to the symmetric and asymmetric stretching vibrations ν(C=C) and the deformation mode δ(N-H). The stretching vibrations ν(C=C) were calculated at about 1582 cm^{-1}. Also, the out of plane deformation mode of δ(NH_2) and in plane deformation mode were calculated as 1526 and 1452 cm^{-1}, respectively. The bands observed at 1348-1040 cm^{-1} correspond to the stretching vibrations of (C-C) (C-H) and δ(C-H) in plane deformation. Bands detected between 967-897 cm^{-1} are attributed to the out of plane deformation mode of δ(C-H). Bands which appear between 760 and 692 cm^{-1} are assigned to the out-of-plane deformation modes of δ (C-N) and δ (C-C). Finally, those observed at 568-497 cm^{-1} are attributed to the mode of deformation of the group δ (C=C) out of the plane.

It is obvious that the theoretical IR spectrum shows a good conformity with the experimental one (Fig.S4).

3.4. Frontier HOMO-LUMO

Fig.6 shows the distributions and energy levels of the HOMO-LUMO orbitals computed at the B3LYP/6-311G(d,p) level for $(C_{10}H_{15}N_2)_2H_2P_2O_7$. The frontier molecular orbitals (FMOs) play an important role in the chemical reactions. The band gap, that is defined as the energy difference between HOMO (the highest occupied molecular orbital), that acts as electron source, and LUMO (the lowest occupied molecular orbital), that acts as electron sink, is a

critical parameters in determining the stability of the structure [35-38]. The HOMO and LUMO energies, the energy gap, the ionization potential (I), the electron affinity (A), electronegativity (χ) softness (S) and the hardness (η) for the $(C_{10}H_{15}N_2)_2H_2P_2O_7$ molecule were calculated at 6-311G(d,p) basis set and the results are given in the Table 6. A hard molecule has a large HOMO-LUMO gap and a soft molecule has a small HOMO-LUMO gap. In the present case the band gap is 3.50 eV and the S parameter was found equal to 0.28 eV. These obtained results (the large value of the band gap and the small S parameter) indicate that the title compound is a hard system which is prone to chemical reactions.

3.5. Mulliken populations analysis

Atomic charges cannot be experimentally obtained because they do not correspond to any physical quantities. Atoms have negatively charged electrons coiled around positively charged nuclei and there are no partial charges on the atoms. But the presence of partial charges on the nucleus results only in the understanding of the electron density distribution. So, Mulliken population method was used to obtain the total atomic charge distributions. Mulliken is highly effective in detecting nucleophilic or electrophilic attacks and regions sensitive to other molecular interactions [39]. The Mulliken charge distributions analysis of molecule was calculated using DFT/B3LYP/6-311G(d,p) level. In Table 7, calculated charges were listed for the title compound. According to Mulliken population analysis results, all hydrogen atoms in the molecule have a positive charge. Mulliken atomic charge values of O8 (-0.689120), O9 (-0.689303), O12 (-0.746854) and O13 (-0.619933) atoms were found to be highly negative values. This is because these atoms are largely electronegative. In addition, it is seen that P3 (1.303282) and P4 (1.242866) atoms has higher Mulliken atomic charge than other positive atoms. The reason for this is that the neighboring atoms (O8, O9, O12 and O13) have significant electronegative properties.

3.6. Molecular electrostatic potential (MEP) surface

The MEP mapped surface of $(C_{10}H_{15}N_2)_2H_2P_2O_7$, for positive and negative potentials, is given in Fig.7. The color code of these maps is in the range between -0.102 a.u. (red) to 0.102 a.u. (blue) for DFT method, the electrostatic potential increases in the order red < orange < yellow < green < blue. The most negative potential (the region where the density of electrons is higher than the nucleus through the whole of the molecule) is shown in red, the blue color is used to indicate the most positive potential (the region of partial positive charges) [40-44]. Interpretation of MEP maps plays a key role in the identification of active sites in chemical bonding and in the synthesis phase of new chemicals. So, to predict reactive sites for electrophilic attack for $(C_{10}H_{15}N_2)_2H_2P_2O_7$, MEP was calculated at the DFT/B3LYP/6-

311G(d,p) optimized geometry. While the negative regions of MEP are rich in electrons, the positive ones are not. This molecule has a possible site for electrophilic attack, as shown in Fig.7, the positive potential sites are around the hydrogen atoms as well as the negative potential sites are localized on the electronegative atoms, the negative regions are mainly over oxygen atoms [O(8), O(9), O(12) and O(13)]. These settlement predicts that O(8), O(9), O(12) and O(13) atoms act as acceptor in hydrogen bonding. As it can be seen, Fig.7 confirms the O–H···O and N–H···O hydrogen bonding in Table 3.

3.7. UV–Vis Absorption

The solid-state UV-Vis absorption spectrum of $(C_{10}H_{15}N_2)_2H_2P_2O_7$ shown in Fig.S5, exhibits two peaks with different intensities and wavelength. The first peak which is located at λ = 330 nm can be attributed to the **π-π*** transition of the phenyl group while the second peak at λ = 380 nm probably may originate from the **n-π*** transition of the diphosphoric anion. The optical band gap Eg, is given by Tauc's model [45] by plotting $(\alpha h\upsilon)^2$ versus $h\upsilon$. This method allows us to classify the sample as a semiconductor with an optical band gap value equal to 2.92 eV (offered by the intersection of the shapely decreasing region with the baseline). This latter allows that the title compound could be used for optical applications in far UV and optoelectronics [46].

3.8. Fluorescence Properties

Fluorescence property of the obtained material have been determined in solid state at room temperature, by choosing the excitation wavelength at λ_{ex} = 330 nm. As seen in Fig.S6 the emission spectrum presents a single peak at λ = 350 nm which is attributed to the intra-ligand **π-π*** of the transition of the 1-phenylpiperazinium cation. To determine fluorescence quantum yield [47] of the synthesized compound, the fluorescence quantum yield of pyrene in cyclohexane (ϕ_f = 0.32) was used as a reference. The fluorescence quantum yield can be calculated using the following equation [48]:

$$\varphi_s = \varphi_f \frac{I_s A_f \eta_s^2}{I_f A_s \eta_r^2}$$

Where φ_f is the fluorescence quantum yield of reference. I stand for the integrated area under the emission curves. The subscripts s and r stand for sample and reference, respectively. A is the absorbance at a particular excitation wavelength. η is the refractive index of the medium. The absorbance of the dye at the excitation wavelength was always kept ~0.1. The steady state absorption and emission spectra were fitted by the log normal line shape function. As a result, the fluorescence quantum yield of 1-phenylpiperazinium

dihydrogenodiphosphate $(C_{10}H_{15}N_2)_2H_2P_2O_7$ is ϕ = 0.54. The compound is relatively high luminescent.

4. Conclusion

Different physico-chemical methods have been used to characterize the novel organic-inorganic hybrid compound $(C_{10}H_{15}N_2)_2H_2P_2O_7$ which have been prepared at room temperature by slow evaporation. The inorganic entities are connected with each other via O–H···O hydrogen bonds and both cations $(C_{10}H_{15}N_2)^+$ and anions $[H_2P_2O_7]^{2-}$ components are held together through N–H···O and C– H···O hydrogen bonds leading to a three dimensional network. The Hirshfeld surface analysis discloses the percentage of intermolecular contacts of the title compound which shows that the H···H interactions are the most abundant (48.4%). The complete vibrational spectral analysis and theoretical calculations were carried out using the density functional theory (DFT/B3LYP) method with 6-311G(d,p). The Mulliken population analysis and the molecular electrostatic potential (MEP) map are supporting each other to give better idea about the chemical active regions. In fact, the result shows that the positive potential sites are around the H atoms. The values of electronegativity, chemical hardness and softness have been calculated. The η and S parameters were found to be 1.75 and 0.28 eV, respectively. The obtained small S parameter indicates that the title compound is a hard system which is prone to chemical reactions. Also, the value of the energy between the HOMO and LUMO was calculated (-3.50 eV). With a large HOMO-LUMO gap we can say that the molecule is hard. The studies of optical and luminescence activities were investigated and in consideration of the results achieved we can confirm the semiconductor behavior of this material with an important band gap energy at 2.92 eV.

Supplementary Data

Crystallographic data for the title compound have been deposited at the Cambridge Crystallographic Data Center as supplementary publication (CCDC 1900203). These data can be obtained free of charge at www.ccdc.cam.ac.uk/conts/retrieving.html (or from the Cambridge Crystallographic Data Center, 12, Union Road, Cambridge CB2 1EZ, UK; fax: +44 1223/336 033; mailto: deposit@ccdc.cam.ac.uk).

Acknowledgements

This work is supported by the Tunisian National Ministry of Higher Education and Scientific Research. A. V. Kindly acknowledges the Academy of Finland (grant no 314343) for financial support.

References:

[1] R. Fezai, A. Mezni, M. Kahlaoui, M. Rzaigui, J. Mol. Struct. 1119 (2016) 54-63.

[2] S. Sleymi, K. Lahbib, N. Rahmouni, M. Rzaigui, S. Besbes-Hentati, S. Abid, J. Mol. Struct. 1144 (2017) 406-414.

[3] S. Kamoun, A. Daoud, R. Von Der Muhll, J. Ravez, Solid State Commun. 85 (1993) 661-664.

[4] J. Zyss, J. Pecaut, J.P. Levy, R. Masse, Acta Cryst.B 49 (1993) 334-342.

[5] J. Pecaut, R. Masse, J. Mater. Chem. 4 (1994) 1851-1854.

[6] F. Hlel, L. Smiri, Solid State Sci. 1 (1999) 321-329.

[7] J.R. Rubin, P. Swaminathan, M. Sundaralingam, Acta Cryst. C 48 (1992) 379-382.

[8] A. Bali, S. Malhotra, H. Dhir, A. Kumar, A. Sharma, Bioorg. Med. Chem. Lett. 19 (2009) 3041-3044.

[9] L. Huang, W. Zhang, X. Zhang, L. Yin, B. Chen, J. Song, Bioorg. Med. Chem. Lett. 25 (2015) 5299-5305.

[10] D.J. Conrado, H. Verli, G. Neves, C.A.M. Fraga, E.J. Barreiro, S.M.K. Rates, T.D. Costa, J. Pharm. Pharmacol. 60 (2008) 699-707.

[11] M.S.R. Murty, K.R. Ram, B.R. Rao, R.V. Rao, M.R. Katiki, J.V. Rao, R. Pamanji, L.R. Velatooru, Med. Chem. Res. 23 (2014) 1661-1671.

[12] N. Jouini, L. BenHamada, A. Jouini, Mater. Res. Bull. 42 (2007) 56-63.

[13] M. Charfi and A. Jouini, Cryst. Res. Technol. 40 (2005) 615-621.

[14] P.N. Prasad, Polym. J. 32 (1991) 1746-1751.

[15] P.A. Franken, A.E. Hill, C.W. Peters, G. Weinreich, Phys. Rev. Lett. 7 (1961) 118-119.

[16] M.W. Klein, C. Enkrich, M. Wegener, S. Linden, Science. 313 (2006) 502-504.

[17] G. Sheldrick, Acta Cryst. A 71 (2015) 3-8.

[18] G.M. Sheldrick, Acta Cryst. C 71 (2015) 3-8.

[19] K. Brandenburg, DIAMOND Version 2.0 (1998).

[20] Gaussian 03, Revision E.01, M.J. Frisch, G.W. Trucks, H.B. Schlegel, G.E. Scuseria, M.A. Robb, J.R. Cheeseman, J.A. Montgomery Jr., T. Vreven, K.N. Kudin, J.C. Burant, J.M. Millam, S.S. Iyengar, J. Tomasi, V. Barone, B. Mennucci, M. Cossi, G. Scalmani, N. Rega, G.A. Petersson, H. Nakatsuji, M. Hada, M. Ehara, K. Toyota, R. Fukuda, J. Hasegawa, M. Ishida, T. Nakajima, Y. Honda, O. Kitao, H. Nakai, M. Klene, X. Li, J.E. Knox, H.P. Hratchian, J.B. Cross, V. Bakken, C. Adamo, J. Jaramillo, R. Gomperts, R.E. Stratmann, O. Yazyev, A.J. Austin, R. Cammi, C. Pomelli, J.W. Ochterski, P.Y. Ayala, K. Morokuma, G.A. Voth, P. Salvador, J.J. Dannenberg, V.G. Zakrzewski, S. Dapprich, A.D. Daniels, M.C.

Strain, O. Farkas, D.K. Malick, A.D. Rabuck, K. Raghavachari, J.B. Foresman, J.V. Ortiz, Q. Cui, A.G. Baboul, S. Clifford, J. Cioslowski, B.B. Stefanov, G. Liu, A. Liashenko, P. Piskorz, I. Komaromi, R.L. Martin, D.J. Fox, T. Keith, M.A. Al- Laham, C.Y. Peng, A. Nanayakkara, M. Challacombe, P.M.W. Gill, B. Johnson, W. Chen, M.W. Wong, C. Gonzalez, J.A. Pople, Gaussian, Inc., Wallingford, CT, 2004.

[21] R. Dennington II, T. Keith, J. Millam, Gauss View, Version 4.1.2, Semichem Inc., Shawnee Mission, KS, 2007.

[22] D. Hartley, H. Kidd (Eds.), The Agrochemicals Handbook, Royal Society of Chemistry/Unwin Brothers Ltd. Old Woking Surrey, United Kingdom (1983).

[23] W. Gerhartz, Ullmann's Encyclopedia of Industrial Chemistry, fifth ed., VCH Publishers, Deerfield Beach FL (1985).

[24] M. P. Andersson, P. Uvdal, J. Phys. Chem. A 109 (2005) 2937-2941.

[25] S. Wolff, D. Grimwood, J. McKinnon, M. Turner, D. Jayatilaka, M. Spackman, Crystal explorer. The University of Western Australia Perth, Australia, 2012.

[26] S. Akriche, M. Rzaigui, Solid State Sci. 2 (2000) 399-405.

[27] W. Baur, Acta Cryst. B 30 (1974) 1195-1215.

[28] D. Cremer, J.A. Pople, J. Am. Chem. Soc. 97 (1975) 1354-1358.

[29] J.J. McKinnon, M.A. Spackman, A.S. Mitchell, Acta Cryst. B 60 (2004) 627-668.

[30] M.A. Spackman, P.G. Byrom, Chem. Phys. Lett. 267 (1997) 215-220.

[31] M. A. Spackman, D. Jayatilaka, Cryst.Eng.Comm 11 (2009) 19-32.

[32] S. Kansiz, N. Dege, Y. Topcu, Y. Atalay, S. V. Gaidai, Acta Cryst.E74 (2018) 1700-1704.

[33] M. Gabelica-Robert, P. Tarte, J. Mol. Struct. 79 (1982) 251-254.

[34] R.W. Mooney, R.L. Goldsmith, J. Inorg. Nucl. Chem 31 (1969) 933-942.

[35] A. Pekparlak, Ö. Tamer, S. D. Kanmazalp, N. Berber, M. Arslan, D. Avcı, N. Dege, E. Tercan, Y. Atalay, J. Mol. Struct. 1171 (2018) 762–770.

[36] S. D. Kanmazalp, M. Macit, N. Dege, J. Mol. Struct. 1179 (2019) 181–191.

[37] S. Kansız, N. Dege, J. Mol. Struct. 1173 (2018) 42–51.

[38] M. K. Gümüş, M. K, S. Kansız, E. Aydemir, N. Y. Gorobets, N. Dege, J. Mol. Struct. 1168 (2018) 280-290.

[39] R. S. Mulliken, J. Chem. Phys. 23 (1955) 1833–1840.

[40] C. C. Ersanli, G. K. Kantar, S. Şaşmaz, J. Mol. Struct. 1143 (2017) 318-327.

[41] Z. Demircioğlu, Ç. Albayrak Kaştaş, O. Büyükgüngör, Spectrochim. Acta, Part A. 139 (2015) 539–548.

[42] F. Şen, S. Kansiz, I. Uçar, Acta Cryst. C73 (2017) 517-524.

[43] S. Demir, M. Dinçer, E. Korkusuz, İ. Yıldırım, J. Mol. Struct. 980 (2010) 1-6.

[44] S. Demir, A. O. Sarioğlu, S. Güler, N. Dege, M. sönmez, J. Mol. Struct. 1118 (2016) 316-324.

[45] J. Tauc, Mater. Res. Bull. 3 (1968) 37-46.

[46] S. Franklin, T. Balasubramanian, K. Nehru, Y. Kim, J. Mol.Struct. 927 (2009) 121-125.

[47] S. E. Braslavsky, Pure Appl. Chem. 79 (2007) 293-465.

[48] C. Würth, M. Grabolle, J. Pauli, M. Spieles, U. Resch-Genger, Nat. Protoc. 8 (2013) 1535-1550.

Table captions

Table 1: Crystal data and structure refinement for $(C_{10}H_{15}N_2)_2H_2P_2O_7$

Table 2: Main interatomic distances (Å) and angles (˚).

Table 3: Principal intermolecular hydrogen bonding geometry (Å, ˚).

Table 4: Some selected geometric parameters for $(C_{10}H_{15}N_2)_2H_2P_2O_7$ (Å, ˚).

Table 5: Comparaison of the observed and calculated vibrational mode frequencies of the title compound.

Table 6: The calculated parameters of $(C_{10}H_{15}N_2)_2H_2P_2O_7$ using DFT/B3LYP/6-311G(d,p) level.

Table 7: Calculated Mulliken charges of the atoms for $(C_{10}H_{15}N_2)_2H_2P_2O_7$.

Table 1

Empirical formula	$(C_{10}H_{15}N_2)_2H_2P_2O_7$
Formula weight	502.43 ($g.mol^{-1}$)
Temperature (K)	170
Wavelength (A ˚)	0.71073
Crystal system	Triclinic
Space group	P1
a (Å) b (Å) c (Å)	5.9159(2) 13.8451(6) 14.5973(5)
α(°) β(°) γ(°)	74.507(2) 89.980(2) 89.231(2)
Volume ($Å^3$)	1152.06(8)
Z	2
D_{calc} ($Mg\ cm^{-3}$)	1.448
Absorption coefficient	0.24 (mm^{-1})
F (000)	532
Theta range for data collection	2.4˚ - 29.2˚
Crystal size (mm^3)	0.25 x 0.22 x 0.04
Limiting indices	$-8<\boldsymbol{h}<7$, $-18<\boldsymbol{k}<18$, $-19<\boldsymbol{l}<19$
Reflections collected	17669
Reflections observed	10693
Goodness-of-fit on F^2	1.02
Final R indices	R_1 = 0.0685 and wR_2 = 0.1478
Largest diff. peak and hole ($e\ Å^{-3}$)	0.76 and -0.40

Table 2

Tétraèdre P(1)O_4:				
P(1)	***O(1)***	***O(2)***	***O(3)***	***O(4)***
O(1)	***1.489 (4)***	*116.1 (3)*	*109.2 (3)*	*110.8 (3)*
O(2)	*2.560(3)*	***1.528 (5)***	*110.6 (3)*	*105.8 (3)*
O(3)	*2.460(2)*	*2.513(1)*	***1.528 (5)***	*103.5 (3)*
O(4)	*2.543(1)*	*2.495(2)*	*2.456(3)*	***1.599 (5)***
Tétraèdre P(2)O_4:				
P(2)	***O(4)***	***O(5)***	***O(6)***	***O(7)***
O(4)	***1.612(5)***	*103.0 (3)*	*103.3 (3)*	*112.4 (3)*
O(5)	*2.443(2)*	***1.509(5)***	*108.4 (3)*	*116.2(3)*
O(6)	*2.471(2)*	*2.472(2)*	***1.538(5)***	*112.3 (3)*
O(7)	*2.592(3)*	*2.559(3)*	*2.529(2)*	***1.506(5)***
Tétraèdre P(3)O_4:				
P(3)	***O(8)***	***O(9)***	***O(10)***	***O(11)***
O(8)	***1.493 (5)***	*115.3(3)*	*108.9 (3)*	*111.0 (3)*
O(9)	*2.554(2)*	***1.529(5)***	*111.0 (3)*	*106.1 (3)*
O(10)	*2.462(3)*	*2.524(2)*	***1.534 (5)***	*104.0 (3)*
O(11)	*2.546(1)*	*2.497(3)*	*2.467(2)*	***1.596 (4)***
Tétraèdre P(4)O_4:				
P(4)	***O(11)***	***O(12)***	***O(13)***	***O(14)***
O(11)	***1.610(5)***	*103.1(2)*	*112.4 (3)*	*102.7 (3)*
O(12)	*2.442(2)*	***1.505(5)***	*116.4 (3)*	*108.1 (3)*
O(13)	*2.593(3)*	*2.562(2)*	***1.510(5)***	*112.8 (3)*
O(14)	*2.461(2)*	*2.466(3)*	*2.541(1)*	***1.540(5)***

P(1)-P(2) 2.943(3) P(1)-O(4)-P(2) 132.9(3)°

P(3)-P(4) 2.937(3) P(3)-O(11)-P(4) 132.7(3)°

P(1)-O(E3)-H(30) = 110° P(2)-O(E6)-H(60) = 108° P(3)-O(E10)-H(100) = 119.9°
P(4)-O(E11)-H(140) = 106°

Table 3

D—H···A	D—H(Å)	H···A(Å)	D···A(Å)	D—H···A(°)
O3—H30···O7^{ii}	0.83 (3)	1.81 (4)	2.585 (7)	155 (8)
O6—H60···O2^{iii}	0.84 (3)	1.73 (4)	2.531 (6)	159 (8)
O10—H100···O13^{iii}	0.82 (3)	1.83 (4)	2.599 (7)	156 (8)
O14—H140···O9^{ii}	0.84 (3)	1.72 (4)	2.524 (7)	159 (9)
N1—H1A···O12	0.91 (3)	1.83 (4)	2.695 (7)	157 (7)
N1—H1B···O1^{i}	0.92 (3)	1.73 (3)	2.651 (7)	176 (7)
N1A—H1C···O5	0.90 (3)	1.80 (3)	2.679 (7)	164 (6)
N1A—H1D···O9^{ii}	0.91 (3)	1.87 (3)	2.770 (7)	174 (6)
N1B—H1E···O5	0.92 (3)	1.82 (4)	2.689 (7)	156 (6)
N1B—H1F···O8	0.91 (3)	1.74 (3)	2.646 (7)	176 (7)
N1C—H1G···O2^{iii}	0.90 (3)	1.87 (3)	2.762 (7)	174 (7)
N1C—H1H···O12^{iv}	0.90 (3)	1.81 (3)	2.687 (8)	162 (6)
C6A—H6D···O8	0.99(1)	2.37(2)	3.295(3)	155(1)
C6C—H6H···O1	0.99(1)	2.39(2)	3.302(3)	153(1)

Symmetry code: (i) *x*, *y*, *z*−1; (ii) *x*+1, *y*, *z*; (iii) *x*−1, *y*, *z*; (iv) *x*, *y*, *z*+1.

Table 4

Geometric Parameters	Experimental [X–ray diffraction]	Calculated DFT
Bond lengths (Å)		
P3─O8	1.493 (5)	1.5092
P3─O9	1.529 (5)	1.5158
P3─O10	1.534 (5)	1.6262
P3─O11	1.596 (4)	1.6542
P4─O11	1.610 (4)	1.6664
P4─O12	1.505 (5)	1.5238
P4─O13	1.510 (5)	1.4894
P4─O14	1.540 (5)	1.6437
N1─C2	1.505 (9)	1.4866
N1─C6	1.474 (9)	1.4893
N4─C3	1.443 (8)	1.4604
N4─C5	1.459 (9)	1.4703
N4─C7	1.407 (8)	1.4188
N1B─C2B	1.507 (9)	1.5012
N1B─C6B	1.469 (8)	1.4919
N4B─C3B	1.428 (8)	1.4592
N4B─C5B	1.474 (8)	1.4734
N4B─C7B	1.405 (8)	1.4185
Bond angles (˚)		
O8─P3─O11	111.0 (3)	109.9153
O9─P3─O11	106.1 (3)	103.9823
O10─P3─O11	104.0 (3)	102.2941
O8─P3─O9	115.3 (3)	120.1388
O12─P4─O11	103.1 (2)	105.4056
O13─P4─O11	112.4 (3)	106.9928
O14─P4─O11	102.7 (3)	101.6897
O12─P4─O13	116.4 (3)	124.2052
P3─O11─P4	132.7 (3)	128.0915
C2─N1─C6	111.7 (5)	112.2355
C3─N4─C5	111.8 (5)	111.5549
C2B─N1B─C6B	112.5 (5)	111.8346
C3B─N4B─C5B	112.1 (5)	111.4292

Table 5

Assignments	Experimental IR (cm^{-1})	Calculated B3LYP/6-311G(d,p)
ν(OH)	-	3702
ν(OH)	-	3373
ν_{ar}(CH)	-	3060
ν_{ar}(CH)	3014	-
$\nu_{as}(CH_2)$	2973	2990
$\nu_{s}(CH_2)$	2920	2932
$\nu_{as}(NH_2)$	2840	2830
$\nu_{s}(NH_2)$	-	1844
$\beta(NH_2)$	1640	1650
ν(C═C)	1607	-
ν(C═C)	-	1582
$\gamma(NH_2)$	1503	1526
β_{ar}(CH)	-	1473
$\beta(CH_2)$	-	1452
$\beta(CH_2)$	1400	-
$\gamma(CH_2)$	1350	1366
$\gamma(CH_2)$	1320	1321
$\gamma(CH_2)$	-	1293
$\nu_{as}(PO_3)$	1255	1248
$\gamma[(CH_2)+ (NH_2)]$	-	1224
$\nu_{as}(PO_3)$	1173	1153
$\gamma[(CH_2)+ (NH_2)]$	-	1137
$\gamma[(CH_2)+ (NH_2)]$	1088	1108
$\gamma[(CH_2)+ (NH_2)]$	1036	-
$\nu_{s}(PO_3)$	-	1004
$\nu_{s}(PO_3)$	974	988
$\beta(NH_2)$	-	933
Ring breathing	900	904
ν_{as}(POP)	-	844
ν_{as}(POP)	760	785
γ_{ar}(CH)	-	745
γ_{ar}(CH)	720	714
ν_{s}(POP)	692	673

υ: stretching; β: in-plane bending; γ: out of plane bending; as: asymmetric, s: symmetric, ar: aromatic

Table 6

Parameters		DFT/B3LYP
HOMO energy	E_{HOMO} (*eV*)	-8.63
LUMO energy	E_{LUMO} (*eV*)	-5.13
Energy gap	$\Delta E = E_{HOMO} - E_{LUMO}$ (*eV*)	-3.50
Iionization potential	$I = -E_{HOMO}$ (*eV*)	8.63
Electron affinity	$A = -E_{LUMO}$ (*eV*)	5.13
Electronegativity	$\chi = (I + A)/2$ (*eV*)	6.88
Hardness	$\eta = (I - A)/2$ (*eV*)	1.75
Softness	$S = 1/2\eta$ (eV^{-1})	0.28

Table 7

Atom	Mulliken Charges	Atom	Mulliken Charges	Atom	Mulliken Charges
P3	1.303282	C7B	0.159211	H3F	0.150134
P4	1.242866	C8	-0.014025	H5A	0.132747
N1	0.263194	C8B	-0.015807	H5B	0.132534
N1B	0.252966	C9	-0.002623	H5E	0.154133
N4	-0.463387	C9B	-0.004424	H5F	0.140936
N4B	-0.469540	C10	-0.000816	H6A	0.169623
O8	-0.689303	C10B	-0.002028	H6B	0.135548
O9	-0.689120	C11	0.000341	H6E	0.125308
O10	-0.266076	C11B	0.000251	H6F	0.215853
O11	-0.755632	C12	0.013687	H8	0.104184
O12	-0.746854	C12B	0.016641	H8B	0.102510
O13	-0.619933	H1A	0.315906	H9	0.094887
O14	-0.265276	H1B	0.340404	H9B	0.093495
C2	0.205690	H1E	0.371701	H10	0.092485
C2B	0.195150	H1F	0.260148	H10B	0.091484
C3	0.187839	H2A	0.152198	H10O	0.291559
C3B	0.201343	H2B	0.140336	H11	0.093747
C5	0.177576	H2E	0.149459	H11B	0.093789
C5B	0.195150	H2F	0.136303	H12	0.094563
C6	0.214580	H3A	0.136865	H12B	0.095711
C6B	0.216808	H3B	0.136865	H14O	0.294926
C7	0.158108	H3E	0.136631		

Figure captions

Figure 1: (a) Atomic arrangement of $(C_{10}H_{15}N_2)_2H_2P_2O_7$ in projection along the a-direction. (b) A view of $[H_2P_2O_7]^{2-}$ anions, projected along the b-axis showing the presence of the rings $R_2^2(8)$, the organic entities are omitted for figure clarity.

Figure 2: Optimized geometry of the molecule.

Figure 3: The red circular collapsing on the d_{norm} surface of $(C_{10}H_{15}N_2)_2H_2P_2O_7$ structure represents the O–H···O, N–H···O and C–H···O intermolecular interactions.

Figure 4: The view of the 2D fingerprint plots with a d_{norm} for (*a*) the sum of the contacts contributing to the Hirshfeld surface, (*b*) H···H (48.4%), (*c*) O···H/H···O (29.6%), (*d*) C···H/H···C (19.3%), (*e*) N···H/H···N (2.2%) and (*f*) C···C (0.3%) contacts in the title compound.

Figure 5: FT-IR spectrum (theoretical and experimental) of $(C_{10}H_{15}N_2)_2H_2P_2O_7$.

Figure 6: Molecular orbital surfaces for the HOMO and LUMO of the title compound computed at B3LYP/6-311G(d,p) level.

Figure 7: The total electron density surface 3D mapped with molecular electrostatic potential (MEP) of the title compound.

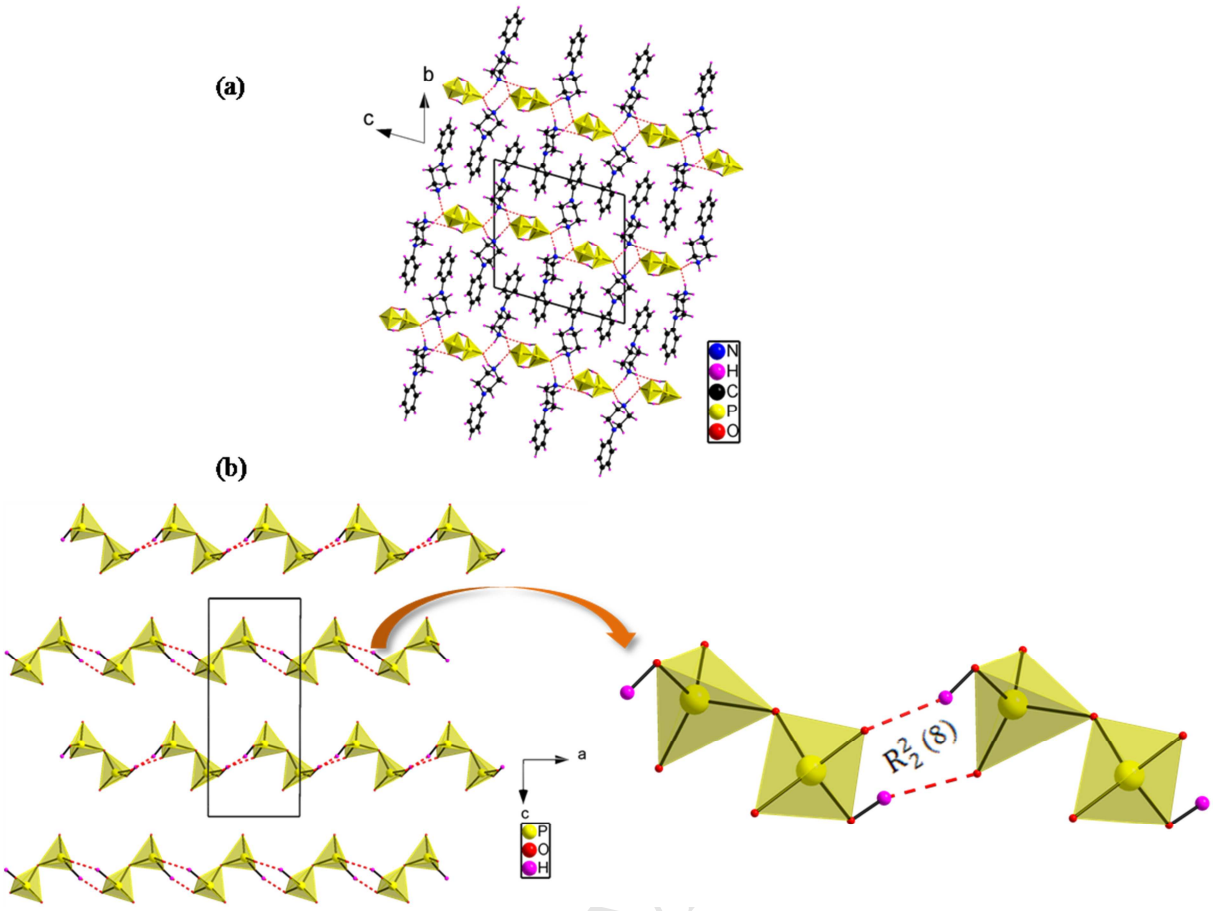

Figure 1

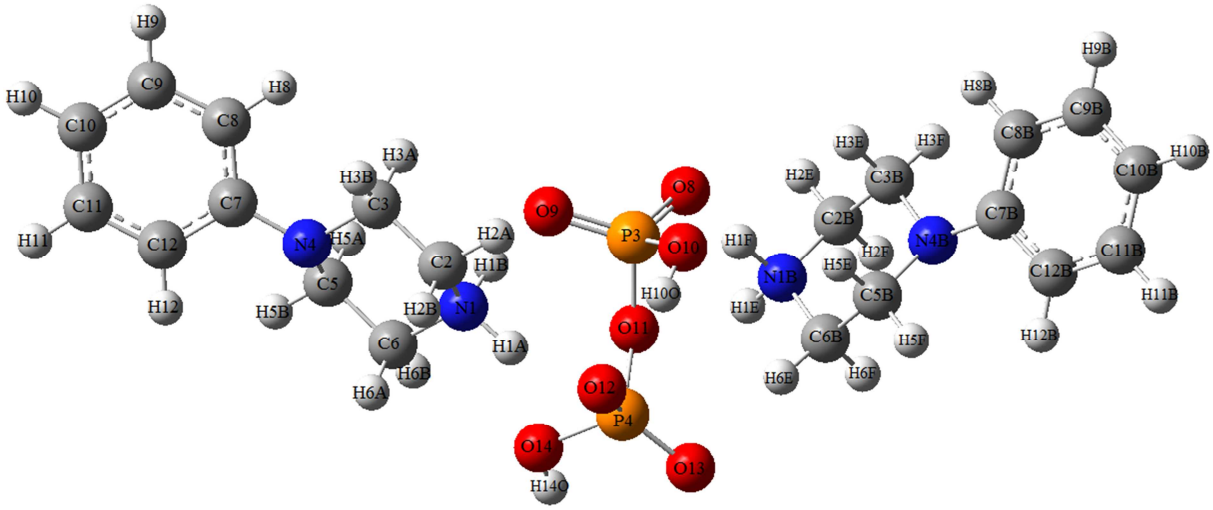

Figure 2

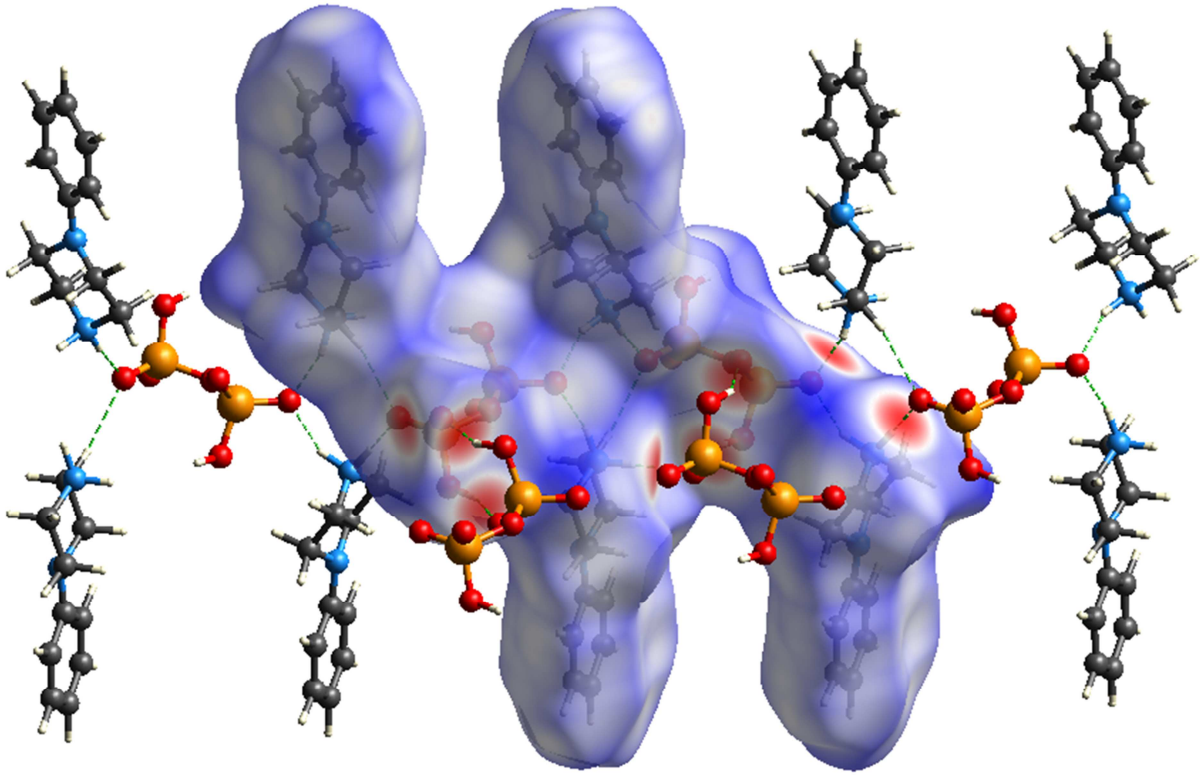

Figure 3

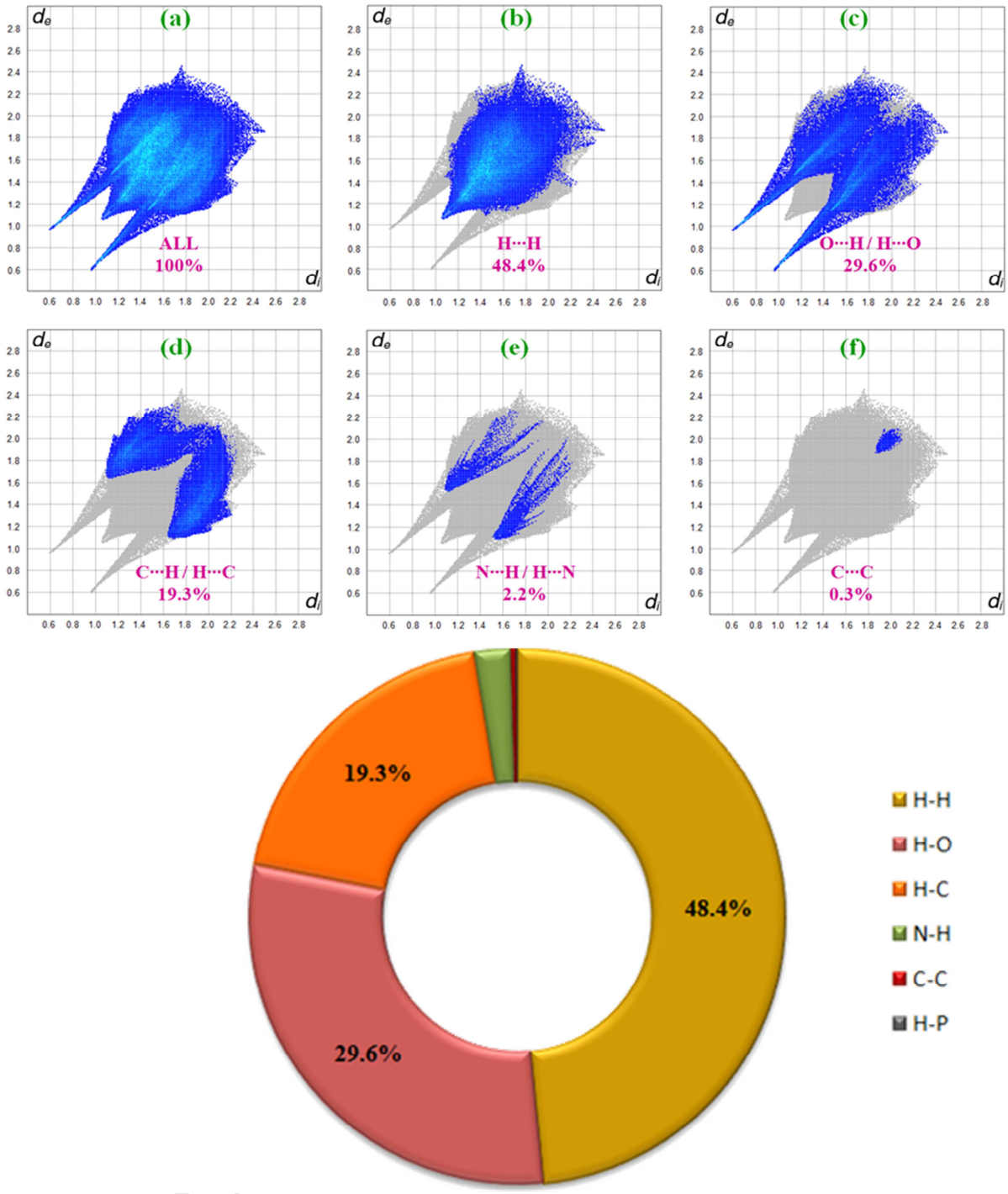
(a)
ALL
100%
(b)
H···H
48.4%
(c)
O···H / H···O
29.6%
(d)
C···H / H···C
19.3%
(e)
N···H / H···N
2.2%
(f)
C···C
0.3%
d_e
d_i
19.3%
48.4%
29.6%
H-H
H-O
H-C
N-H
C-C
H-P

Figure 4

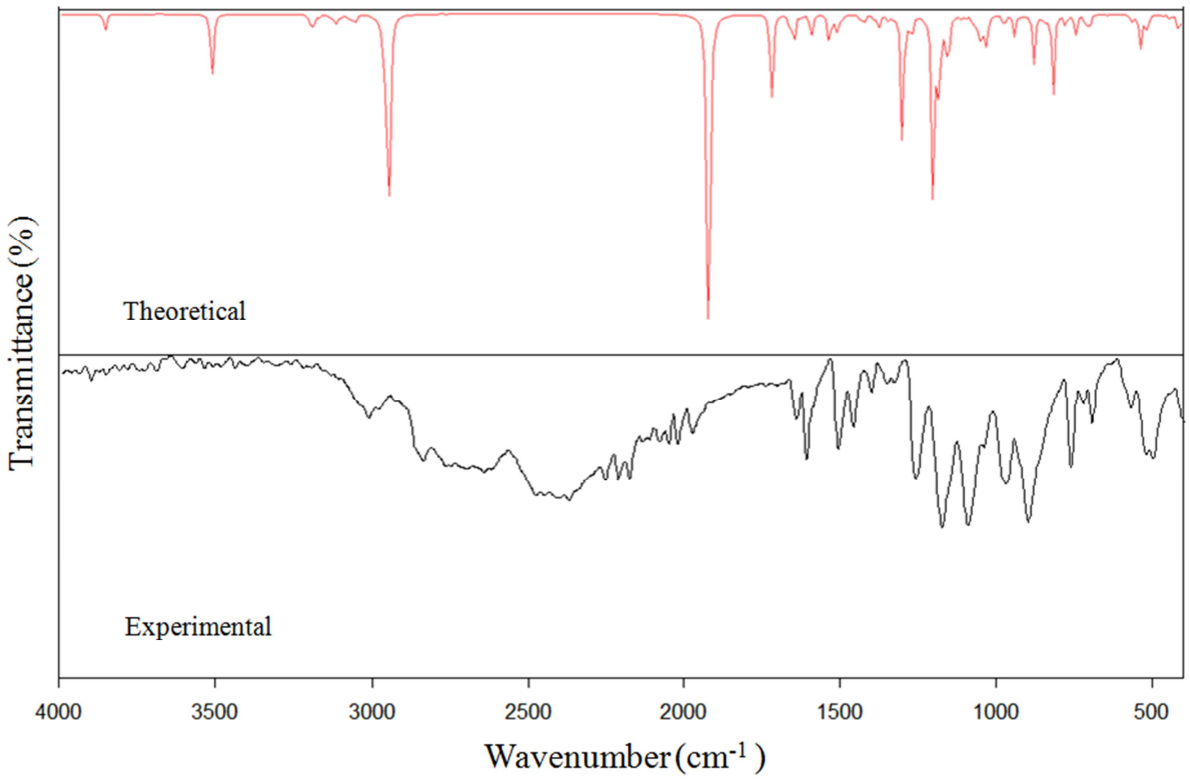

Figure 5

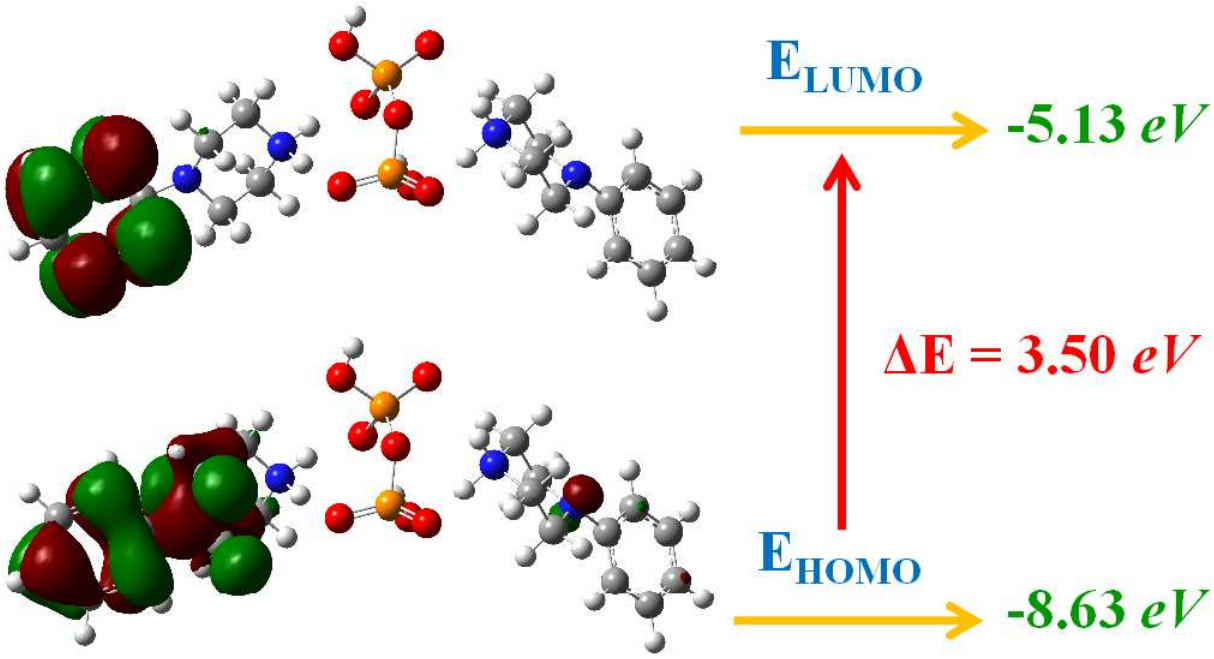

Figure 6

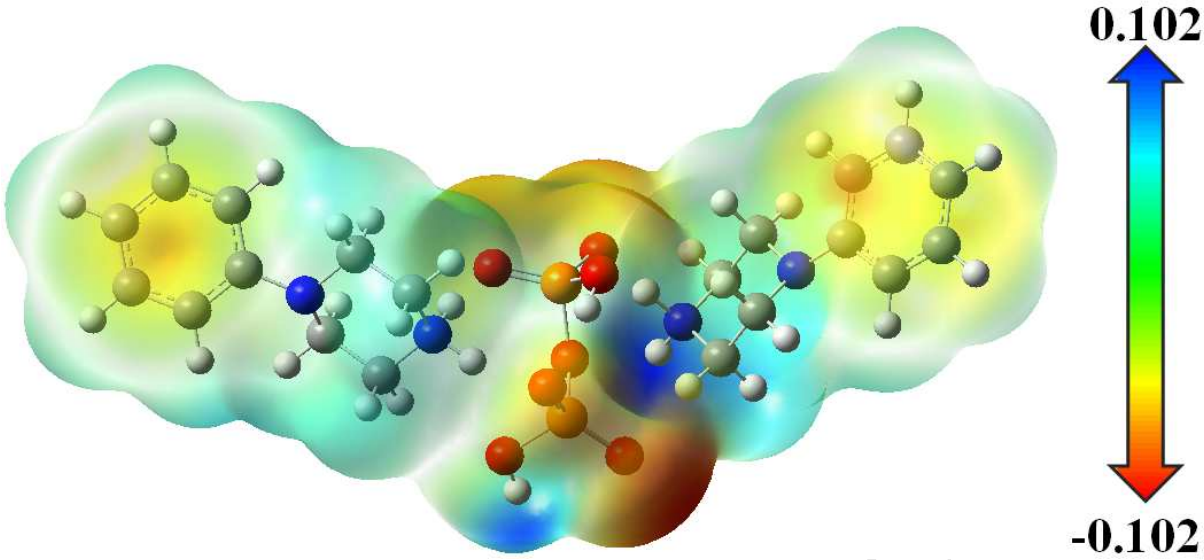

Figure 7

Highlights

- ✓ A new organic-inorganic diphosphate was synthesized at room temperature.
- ✓ The XRPD data confirms the phase purity of the non-centrosymmetric material $(C_{10}H_{15}N_2)_2H_2P_2O_7$.
- ✓ Hirshfeld surface analysis was used to evaluate intermolecular contacts.
- ✓ The computed vibrational spectra are in good agreement with the experimental results.
- ✓ HOMO-LUMO, Mulliken population and MEP were reported.
- ✓ Optical absorption and luminescence measurements were studied.